Statistical properties of ^{243}Pu, and ^{242}Pu(n,γ) cross section calculation

T. A. Laplace,[1,2,*] F. Zeiser,[3] M. Guttormsen,[3] A. C. Larsen,[3] D. L. Bleuel,[1] L. A. Bernstein,[1,2,4] B. L. Goldblum,[2] S. Siem,[3]
F. L. Bello Garrote,[3] J. A. Brown,[2] L. Crespo Campo,[3] T. K. Eriksen,[3] F. Giacoppo,[3] A. Görgen,[3] K. Hadyńska-Klęk,[3]
R. A. Henderson,[1] M. Klintefjord,[3] M. Lebois,[5] T. Renstrøm,[3] S. J. Rose,[3] E. Sahin,[3] T. G. Tornyi,[3] G. M. Tveten,[3] A. Voinov,[6]
M. Wiedeking,[7] J. N. Wilson,[5] and W. Younes[1]

[1]*Lawrence Livermore National Laboratory, Livermore, California 94551, USA*
[2]*Department of Nuclear Engineering, University of California, Berkeley, California 94720, USA*
[3]*Department of Physics, University of Oslo, N-0316 Oslo, Norway*
[4]*Lawrence Berkeley National Laboratory, Berkeley, California 94720, USA*
[5]*Institut de Physique Nucléaire d'Orsay, Bât. 100, 15 rue G. Clemenceau, 91406 Orsay Cedex, France*
[6]*Department of Physics and Astronomy, Ohio University, Athens, Ohio 45701, USA*
[7]*iThemba LABS, P.O. Box 722, Somerset West 7129, South Africa*

The level density and γ-ray strength function (γSF) of ^{243}Pu have been measured in the quasicontinuum using the Oslo method. Excited states in ^{243}Pu were populated using the ^{242}Pu(d,p) reaction. The level density closely follows the constant-temperature level density formula for excitation energies above the pairing gap. The γSF displays a double-humped resonance at low energy as also seen in previous investigations of actinide isotopes. The structure is interpreted as the scissors resonance and has a centroid of $\omega_{SR} = 2.42(5)$ MeV and a total strength of $B_{SR} = 10.1(15)$ μ_N^2, which is in excellent agreement with sum-rule estimates. The measured level density and γSF were used to calculate the ^{242}Pu(n,γ) cross section in a neutron energy range for which there were previously no measured data.

I. INTRODUCTION

Neutron capture cross sections are required for the accurate modeling of advanced nuclear energy systems and nucleosynthesis in neutron-rich astrophysical environments. Unfortunately, it is often difficult to accurately measure (n,γ) cross sections for short-lived "minor" actinides over the energy range of greatest relevance to nuclear energy and astrophysical applications. In these cases an alternative approach is to measure the properties of excited nuclear states, including the nuclear level density and γ-ray strength function (γSF), and use these as inputs for calculations of neutron capture reaction rates using statistical model codes. In this paper we are concentrating on the properties of the $n + {}^{242}$Pu compound system.

With a half-life of 0.37 million years, ^{242}Pu is the second longest-lived isotope of Pu after ^{244}Pu. Though its radioactivity is not one of the largest contributors to nuclear waste decay heat, ^{242}Pu is fissionable by fast neutrons and can be recycled in fast reactors. With the increase of the fuel cycle length and the development of fast reactors aimed at reducing radioactive waste comes the need for reliable cross sections for a fast neutron spectrum [1,2]. It is extremely important to be able to accurately predict cross sections where measured data are insufficient or nonexistent.

Furthermore, improvements in the modeled reaction rates could also improve predictions of actinide abundances on Earth [3]. Actinides are synthesized in extreme stellar environments uniquely by the rapid neutron capture process [3]. For accurate predictions, reactions rates for actinides with high neutron excess are the most crucial. However, such actinide isotopes with extreme neutron-to-proton ratios are out of reach experimentally, and will remain so for many years to come. Thus, it is imperative to obtain a better understanding of the fundamental nuclear properties in this mass region, to provide stringent test on nuclear models invoked to calculate these reaction rates [3].

Measurements of the statistical properties of the nucleus are important for nuclear cross section calculations in the framework of the statistical model. The nuclear level density and γSF can be extracted using the Oslo method [4,5]. This method has been successfully applied recently in the actinide region to the $^{231-233}$Th, ^{232,233}Pa, $^{237-239}$U, and ^{238}Np isotopes [6–9]. Thus far, the level densities of all measured actinides follow closely the constant-temperature level density formula. These heavy and well-deformed systems also show a low energy orbital $M1$ scissors resonance (SR). The main purpose of the present work is to extract the level density and γSF in ^{243}Pu. Comparing the measured to an estimated γSF, the SR is extracted and interpreted as an enhancement of the γSF. Hauser-Feshbach calculations of the neutron capture cross section using the measured level density and γSF as inputs are compared with evaluated nuclear databases.

In Sec. II the experimental procedure is described. Section III discusses the extraction and normalization of the level density and γSF. In Sec. IV, the experimental SR is presented and theoretical sum rules are briefly introduced. Extracted resonance parameters are compared to previous results and sum-rules estimates. In Sec. V, the measured level density and γSF are used as inputs to Hauser-Feshbach calculations in order to estimate the ^{242}Pu(n,γ) cross sections. Conclusions are drawn in Sec. VI.
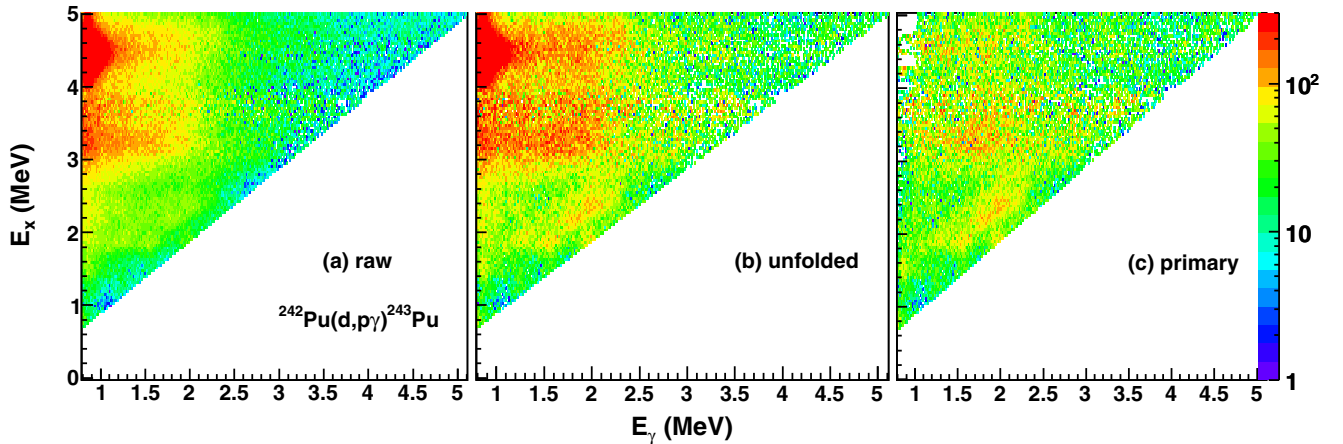
*lapthi@berkeley.edu

FIG. 1. Initial excitation energy E_x versus γ-ray energy E_γ from particle-γ coincidences recorded from the ^{242}Pu$(d,p\gamma)^{243}$Pu reaction. The raw γ-ray spectra (a) are first unfolded (b) by the NaI response function. The primary or first-generation γ-ray spectra (c) are extracted as function of excitation energy E_x.

II. EXPERIMENTAL METHODS

The experiment was conducted using the MC-35 Scanditronix cyclotron at the Oslo Cyclotron Laboratory (OCL). The 0.4 mg/cm^2 ^{242}Pu on a Be-backing target was bombarded with a 12 MeV deuteron beam with a beam current of ≈ 1 nA. Prior to electrodeposition, the Pu material was cleaned from decay products and other impurities using an anion-exchange resin column procedure [10]. The purified product was electroplated onto a thin Be foil (1.9 mg/cm^2 thickness) from a small aliquot of dilute nitric acid placed into a large volume of isopropanol. The resulting target was dried, baked at 500°C in a muffle furnace, then glued to the target frame.

Particle-γ coincidences were measured using the SiRi particle telescope and the CACTUS γ-detector system [11,12]. The SiRi particle telescope is composed of eight segmented Si particle telescopes, which in this experiment were placed at backward angles of $\theta = 126°$ to $140°$ relative to the beam axis, drastically reducing the contribution from elastically scattered deuterons. The resulting spin distribution of the nucleus is more representative of the compound nuclei formed in higher-energy (e.g., nonthermal) (n,x) reactions. Each telescope is comprised of a ΔE and E Si detector with thicknesses of 130 μm and 1550 μm, respectively. The CACTUS array consists of 26 collimated 5 in. $\times$ 5 in. NaI(Tl) detectors surrounding the target and particle telescopes, and with a total efficiency of 14.1(2)% at $E_\gamma = 1.33$ MeV.

The particle telescopes were used to generate the master gate signal and the start signal for the time-to-digital converters (TDC). The NaI detectors were used as individual TDC stops. Thus prompt particle-γ coincidences with background subtraction were sorted event by event. The proton events were extracted by setting proper two-dimensional gates on the ΔE-E matrices. Using the measured proton energies deposited in the telescopes and the reaction Q value, the initial excitation energy E_x in the residual ^{243}Pu nucleus was calculated. To avoid contamination from γ rays emitted by other reaction channels, only excitation energies below the

fission barrier ($B_f \approx 6$ MeV [13]) and the neutron separation energy ($S_n = 5.034$ MeV [14]) were considered.

The recorded particle-γ coincident events were sorted into a two-dimensional matrix as shown in Fig. 1(a). Using the known response function of the CACTUS array, the raw data were unfolded to correct for the NaI response functions and efficiency, and regain the full-energy peaks for each 40 keV excitation energy bin [15]. The unfolded matrix is shown in Fig. 1(b). A peak at $E_\gamma = 870$ keV from O contamination was subtracted from the matrix.

The Oslo method was used to extract the first generation (primary) γ rays from the total γ-ray cascade [16]. The main assumption in the technique is that γ decay from a given excitation energy is independent on how the nucleus was excited [e.g., directly via (d,p) reactions or from γ decay from a higher-lying level]. The first-generation γ-ray matrix $P(E_x, E_\gamma)$ is shown in Fig. 1(c).

Figure 2 shows the average γ-ray multiplicity $\langle M_\gamma(E_x) \rangle$ for $E_\gamma > 0.4$ MeV as function of initial excitation energy E_8 given by

$$\langle M_\gamma(E_x) \rangle = \frac{E_x}{\langle E_\gamma(E_x) \rangle}, \qquad (1)$$

where the average γ-ray energy $\langle E_\gamma(E_x) \rangle$ is calculated from the unfolded γ matrix at a fixed excitation energy E_x.

Below $E_x = 2$ MeV, the multiplicity fluctuates indicating a nonstatistical behavior of the decay process while approaching the ground state. Above $E_x = 4.5$–5 MeV, the multiplicity fluctuates due to the opening of the fission and neutron emission channels. To apply the Oslo method, only the $E_x = 2.6$–4.3 MeV region of the first generation matrix of Fig. 1(c) is used.

Fermi's golden rule [17] states that the decay probability can be factorized into a transition matrix element between the initial and final state and the density of final states. According to Brink's hypothesis [18], the transmission coefficient $\mathcal{T}$, which plays the role of the transition matrix element in Fermi's Golden rule, is independent of the excitation energy. The first
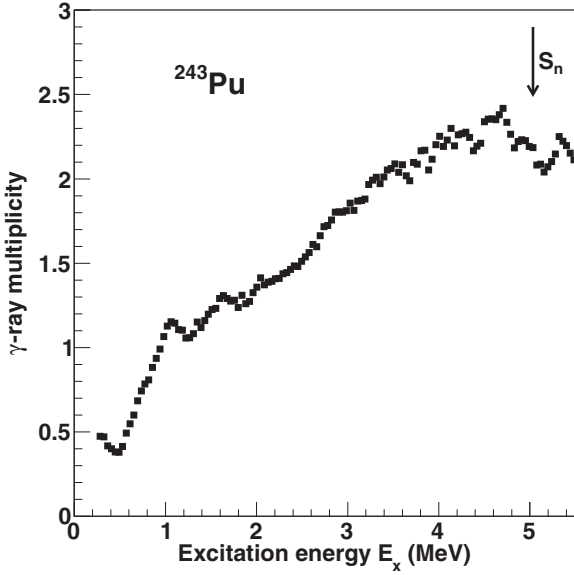
FIG. 2. γ-ray multiplicity as function of excitation energy E_x in ^{243}Pu. Only γ rays with $E_\gamma > 0.4$ MeV are taken into account.

generation matrix $P(E_x, E_\gamma)$ can be factorized as follows:

$$P(E_x, E_\gamma) \propto \mathscr{T}(E_\gamma)\rho(E_x - E_\gamma), \qquad (2)$$

where $\rho(E_x - E_\gamma)$ is the level density at the excitation energy after the primary γ ray has been emitted in the cascades. Simultaneous extraction of the level density and the γ-ray transmission coefficient is achieved using an iterative procedure to the first generation matrix $P(E_x, E_\gamma)$ [4]. It has been shown [4] that if one solution for the multiplicative functions ρ and $\mathscr{T}$ is known, one may construct an infinite number of transformations $\tilde{\rho}$ and $\tilde{\mathscr{T}}$, which give identical fits to the $P(E_x, E_\gamma)$ matrix by

$$\tilde{\rho}(E_x - E_\gamma) = A \exp[\alpha(E_x - E_\gamma)]\, \rho(E_x - E_\gamma), \quad (3)$$

$$\tilde{\mathscr{T}}(E_\gamma) = B \exp(\alpha E_\gamma)\mathscr{T}(E_\gamma), \qquad (4)$$

where the parameters A, α, and B cannot be determined by the fitting procedure. Their determination is discussed in the next section.

III. NORMALIZATION OF THE LEVEL DENSITY AND γSF

The parameters A and α of Eq. (3) are needed to obtain a normalized level density. They can be determined by matching the data points at low energy to known discrete levels [19] and estimating the level density at the neutron separation energy S_n from neutron-resonance spacing data using the formula [4]

$$\rho(S_n) = \frac{2\sigma^2}{D_0}$$
$$\cdot \frac{1}{(I_t+1)\exp[-(I_t+1)^2/2\sigma^2]+I_t\exp\left[-I_t^2/2\sigma^2\right]},$$
$$(5)$$

where I_t is the spin of the target nucleus, D_0 the neutron resonance spacing, and σ the spin-cutoff parameter. The

following spin distribution is assumed [20] in the produced nucleus:

$$g(E_x = S_n, I) \simeq \frac{2I+1}{2\sigma^2}\exp[-(I+1/2)^2/2\sigma^2], \quad (6)$$

where I is the spin in the resulting nucleus. The spin-cutoff parameter σ was determined from the global systematic study of level-density parameters by von Egidy and Bucurescu, using a rigid-body moment of inertia approach [21]:

$$\sigma^2 = 0.0146A^{5/3}\frac{1+\sqrt{1+4aU}}{2a}, \qquad (7)$$

where A is the mass number, a is the level density parameter, $U = E_x - E_1$ is the intrinsic excitation energy, and E_1 is the back-shift parameter. The a and E_1 parameters are obtained from global systematics. Table I lists the parameters used to estimate σ. From the deduced σ value and D_0 at S_n the level density ρ is determined. Several values for D_0 were reported in the literature: RIPL-3 [$D_0 = 13.5(15)$ eV] [13], Mughabghab [$D_0 = 17(1)$ eV] [22], Young and Reeder [$D_0 = 16.5$ eV] [23], and Rich *et al.*, using the ESTIMA code [$D_0 = 16.8(5)$ eV] [24]. The RIPL-3 [13] value is inconsistent with other works. Normalization of the level density and the γSF was performed using the different values and using $D_0 = 17(1)$ eV provided a more consistent result with a measurement on a ^{240}Pu target made at the same facility [25]. Thus, to obtain the level density at S_n given in Table I, the D_0 parameter is taken from Ref. [22]. In order to perform the normalization at S_n, the constant-temperature formula [26] is used for the interpolation of our experimental data points and the level density at S_n:

$$\rho_{\mathrm{CT}}(E_x) = \frac{1}{T_{\mathrm{CT}}}\exp\frac{E_x - E_0}{T_{\mathrm{CT}}}. \qquad (8)$$

The slope of the level density is given by $T_{\mathrm{CT}} = 0.40(1)$ MeV and the shift in excitation energy by $E_0 = -0.95(16)$ MeV. Figure 3 shows the level density normalized at low and high excitation energies. The level density follows closely the constant-temperature formula with $\ln \rho \propto E_x/T_{\mathrm{CT}}$ between $E_x \approx 2$ MeV and $E_x \approx 3$ MeV as observed for other actinide nuclei [7,9]. The Fermi-gas model does not describe properly the data as described in Ref. [27].

The standard procedure to normalize the level density and γSF is problematic when a (d,p) entrance channel is employed in actinides to form the compound nucleus. The spin distribution in the compound nucleus populated using the (d,p) is not as broad as for other reactions such as $(^3\mathrm{He},\alpha)$ which can bring in more angular momentum. As the slope, α, of the transmission coefficient is the same for the level density in Eqs. (3) and (4), a reduced level density ρ_{red} corresponding to the level density for the spins populated in the (d,p) reaction was used to obtain the correct slope of $\mathscr{T}$. The reduced level density thus is extracted by assuming a lower value of ρ at S_n. This effect has been demonstrated in simulated data using DICEBOX on the case of ^{163}Dy [5], where a restriction on the spin of the initial levels was made ($1/2 \leqslant I_{\mathrm{initial}} \leqslant 13/2$). To obtain a correct slope of the transmission coefficient, and thus the γSF extracted from the simulated data (see Figs. 19–21 in Ref. [5]), the level density had to be normalized not to the full level density, but to the reduced level density for spins

TABLE I. Parameters used to extract level density and γSF (see text).

S_n (MeV)	a (MeV^{-1})	E_1 (MeV)	$\sigma(S_n)$	D_0 (eV)	$\rho(S_n)$ (10^6 MeV^{-1})	$\rho(S_n)_{\text{red}}$ (10^6 MeV^{-1})	$\langle\Gamma_\gamma(S_n)\rangle$ (meV)
5.034	25.82[a]	−0.45[a]	8.15[a]	17(1)[b]	7.87(163)	3.94	22(1)[b]

[a]Estimated from systematics [21].
[b]Reference [22].

within the range $1/2 \leqslant I_{\text{final}} \leqslant 15/2$ (one primary transition of dipole type accounts for $I_{\text{final}} = 15/2$).

Cumulating large uncertainties in the total $\rho(S_n)$ and the unknown actual spin distribution brought into the nuclear system by the specific (d,p) reaction, the extracted slope of $\mathscr{T}$ becomes rather uncertain. Those complications encountered using the (d,p) reaction on actinides make the standard normalization procedure of the Oslo method [4,28] to determine the α parameter for the transmission coefficient in Eq. (4) quite uncertain.

The determination of the parameter B of Eq. (4) gives the absolute normalization of $\mathscr{T}$. The average total radiative width $\langle\Gamma_\gamma\rangle$ at S_n, assuming that the γ decay in the continuum is dominated by dipole transitions, is used here for normalization. The width is related to the transmission coefficient $\mathscr{T}$ by [29]

$$\langle\Gamma_\gamma\rangle = \frac{1}{2\pi\rho(S_n,I,\pi)}\sum_{I_f}\int_0^{S_n} dE_\gamma\, B\mathscr{T}(E_\gamma)\rho(S_n - E_\gamma, I_f),$$
(9)

where I and π are the initial spin and parity at S_n, respectively. The summation and integration is performed over

FIG. 3. Level density for ^{243}Pu. At low excitation energy E_x, the experimental data are normalized to the level density of known discrete levels (red solid line). At the neutron separation energy $S_n = 5.038$ MeV, the normalization is done using the level density extracted from known neutron resonance spacings D_0. The connection between $\rho(S_n)$ (the upper right data point) and the experimental data is made with a constant-temperature formula with $T_{\text{CT}} = 0.40(1)$ MeV.

all final levels with spin I_f that are accessible by $E1$ or $M1$ transitions with energy E_γ. The determination of B using Eq. (9) is influenced by systematic errors because the integral depends on both the level density $\rho(E_x)$ and the spin-cutoff parameter $\sigma(E_x)$; the latter quantity is not well constrained experimentally for all excitation energies. Given these complications, we have compared the γSF with the extrapolation of known photonuclear reaction at a, in addition to determining the B parameter using Eq. (9) to reproduce the experimentally determined γ-width $\langle\Gamma_\gamma\rangle$ [22] listed in Table I. Hence, by making use of an independent experimental constraint, we reduce the systematic uncertainties in the absolute normalization of the γSF.

Given these complications, a different procedure is used, comparing the γSF with the extrapolation of known photonuclear reaction data. The strength function is related to the transmission coefficient $\mathscr{T}(E_\gamma)$ by [13]

$$f(E_\gamma) \approx \frac{1}{2\pi}\frac{\mathscr{T}(E_\gamma)}{E_\gamma^3}.$$
(10)

These data are compared with the strength function derived from the cross section σ of photonuclear reactions by [13]

$$f(E_\gamma) = \frac{1}{3\pi^2\hbar^2 c^2}\frac{\sigma(E_\gamma)}{E_\gamma},$$
(11)

where the factor $1/3\pi^2\hbar^2 c^2 = 8.6737 \times 10^{-8}$ mb^{-1}MeV^{-2}.

In Fig. 4 the γSF derived from ^{239}Pu(γ,x) cross sections by Berman *et al.* [30], Gurevitch *et al.* [31], and Moraes *et al.* [32] are shown. There are no measured γSF data for other Pu isotopes. It is assumed that the $E1$ strength does not vary much from ^{239}Pu to ^{243}Pu, as seen for similar mass U isotopes [8], and supported by the classical Thomas-Reiche-Kuhn sum rule for $E1$ strength [33–35].

The data from the present work cover γ energies up to 4.3 MeV while for the (γ, x) data, the lowest energy point is 6.7 MeV. Some interpolation is needed to link the different data sets. The GEDR displays a double-humped feature common to all well-deformed nuclei that is fitted with two enhanced generalized Lorentzians (EGLO) as defined in RIPL [13], but with a constant-temperature parameter of the final states T_f, in accordance with the Brink hypothesis. To take into account the steep rise of our γSF data from $E_\gamma = 3$–4 MeV, a resonance is postulated at around 4.4 MeV (labeled pygmy1 in Fig. 4). Due to the absence of data between 4.3 MeV and 6.7 MeV, the parameters of the resonance are highly uncertain. In addition, the (γ, x) data [32] reveal a knee at around 7.5 MeV indicating an additional resonance-like structure (labeled pygmy2 in Fig. 4). The two pygmy resonances are described by standard
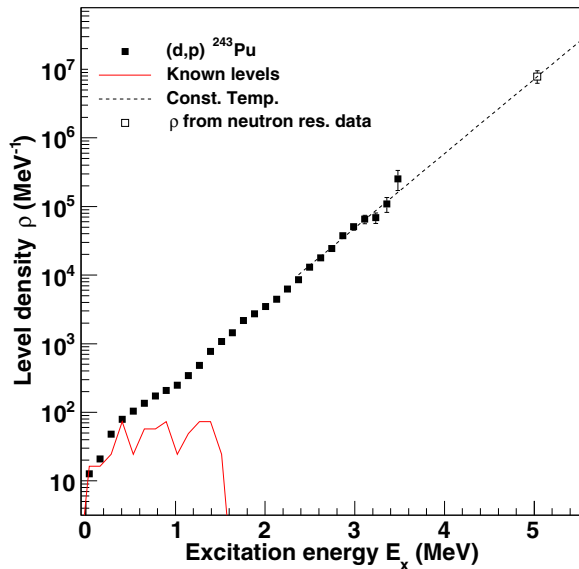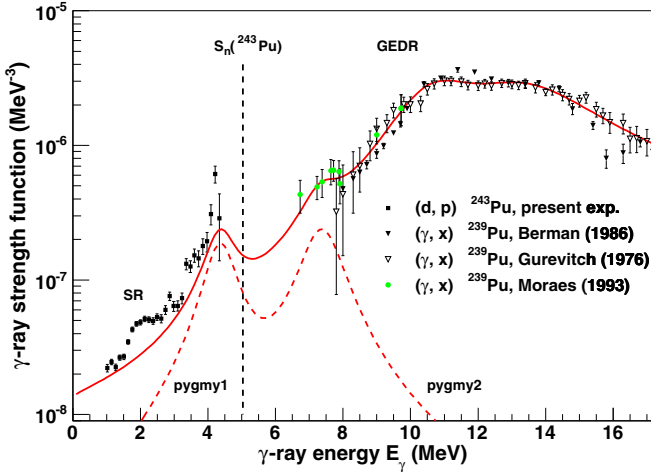
FIG. 4. Experimental γSF from the present $(d, p\gamma)^{243}$Pu experiment (black filled squares) and (γ, x) data (black filled triangles, empty triangles, and green dots) taken, respectively, from Berman *et al.* [30], Gurevitch *et al.* [31], and Moraes *et al.* [32]. The red curve represents the estimated underlying $E1$ part of the γSF. The structure in the present work at $E_\gamma = 1$–3.5 MeV is interpreted as the scissors resonance.

Lorentzians:

$$f_{\mathrm{pyg}} = \frac{1}{3\pi^2\hbar^2c^2} \frac{\sigma_{\mathrm{pyg}}\Gamma_{\mathrm{pyg}}^2 E_\gamma}{\left(E_\gamma^2 - \omega_{\mathrm{pyg}}^2\right)^2 + \Gamma_{\mathrm{pyg}}^2 E_\gamma^2}, \qquad (12)$$

where σ_{pyg}, Γ_{pyg}, ω_{pyg} are the strength, width, and energy centroid of the pygmy resonance, respectively.

The red curve in Fig. 4 is the sum of the GEDR and the two pygmy resonances. It serves as a "base line" of the γSF with no additional strength from other resonances. The parameters for the GEDR and the two pygmy resonances are given in Table II. The measured γSF is normalized to this underlying $E1$ strength. To match the slope of the observed γSF with the GEDR low-energy tail, the level density at S_n was reduced from 7.87 to 3.94 million levels per MeV thereby varying the α parameter from Eq. (3). Calculations of the spin population using the EMPIRE code [36] suggest a reduced level density $\rho_{\mathrm{red}} = 0.34(4) \times \rho$ for ^{243}Pu, ^{233}Th, and ^{238}Np. which were all produced using a 12 MeV deuteron beam. Because the experimental level densities of ^{232}Th and ^{237}Np were reduced by a factor of $\approx 1/2$ [8,9], the same reduction factor was used.

IV. THE SCISSORS RESONANCE AND SUM RULES

Figure 5 shows a γSF measured above the expected γSF base line (red curve in Fig. 4). The extra strength between
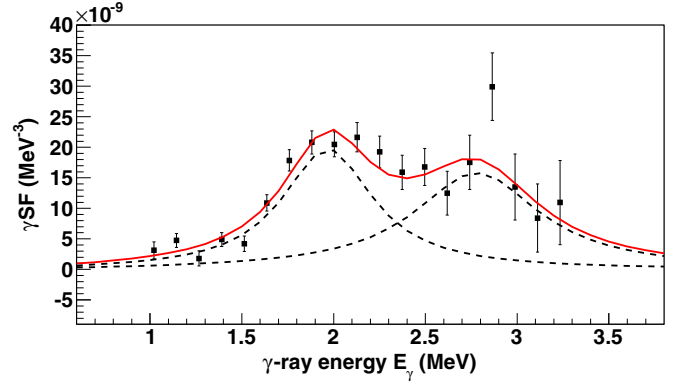

FIG. 5. The extracted γSF for the scissors resonance in the quasicontinuum of ^{243}Pu.

$E_\gamma = 1$ and 3.5 MeV is interpreted as the "scissors" resonance (SR). A similar structure has been previously observed in the $^{231–233}$Th, ^{232,233}Pa, $^{237–239}$U, and ^{238}Np isotopes [6–9]. Even though the parameters of the resonance postulated at 4.5 MeV are rather uncertain, the SR is extracted by subtracting a smoothly varying background under the γSF which is mainly composed of the temperature-dependent low energy tail of the GEDR, as described in the previous section. The SR has been fitted with two Lorentzians. The resonance centroid ω_i, cross section σ_i, and width Γ_i for the lower ($i = 1$) and upper ($i = 2$) resonances are listed in Table III, as well as the total strength and average energy centroid.

The separation between the two components, $\Delta\omega_{\mathrm{SR}} = 0.81(6)$ MeV, is similar to what has been observed for Th, Pa, and U [8] [$\Delta\omega_{\mathrm{SR}} = 0.89(15)$ MeV] and higher than the ^{238}Np observation, $\Delta\omega_{\mathrm{SR}} = 0.53(6)$ MeV [9].

Recent microscopic calculations revealed that the SR contains two modes [37], which could explain the splitting seen experimentally in the actinides. The traditional mode consists of protons oscillating against neutrons and a new "nuclear spin scissors mode" consisting of oscillations of nucleons with the spin projection "up" against nucleons with the spin projection "down". The latest calculations include spin degrees of freedom and pairing, and show good agreement with experimental data for rare earth nuclei.

Calculations using the sum-rule approach [38], were made to predict both the centroid ω_{SR} and strength B_{SR} of the scissors mode. The description of Enders *et al.* [39] was followed. The ground-state moment of inertia was replaced by the rigid-body moment of inertia. The sum rule for the quasicontinuum was recently presented [8], and a detailed description of the formulas and parameters used for ^{238}Np is given in Ref. [9]. The same approach has been applied here. The inversely and

TABLE II. Resonance parameters used for the γSF extrapolation.

$\omega_{E1,1}$ (MeV)	$\sigma_{E1,1}$ (mb)	$\Gamma_{E1,1}$ (MeV)	$\omega_{E1,2}$ (MeV)	$\sigma_{E1,2}$ (mb)	$\Gamma_{E1,2}$ (MeV)	T_f (MeV)	ω_{pyg1} (MeV)	σ_{pyg1} (mb)	Γ_{pyg1} (MeV)	ω_{pyg2} (MeV)	σ_{pyg2} (mb)	Γ_{pyg2} (MeV)
11.1	290	3.2	14.2	340	5.5	0.40(1)	4.4(1)	9(3)	1.0(2)	7.4(3)	20(6)	1.3(3)

TABLE III. Scissors resonance parameters for ^{243}Pu and sum-rule estimates.

Deformation	Lower resonance				Upper resonance				Total		Sum rule	
δ	$\omega_{SR,1}$ (MeV)	$\sigma_{SR,1}$ (mb)	$\Gamma_{SR,1}$ (MeV)	$B_{SR,1}$ (μ_N^2)	$\omega_{SR,2}$ (MeV)	$\sigma_{SR,2}$ (mb)	$\Gamma_{SR,2}$ (MeV)	$B_{SR,2}$ (μ_N^2)	ω_{SR} (MeV)	B_{SR} (μ_N^2)	ω_{SR} (MeV)	B_{SR} (μ_N^2)
0.27[a]	1.99(4)	0.45(6)	0.60(8)	4.8(9)	2.81(5)	0.51(8)	0.83(14)	5.3(12)	2.42(5)	10.1(15)	2.3	10.6

[a]Average of calculations using the ground state deformation parameter β_2 from Refs. [13,40].

linearly energy-weighted sum rules are given by [8]

$$S_{+1} = \frac{3}{2\pi}\Theta_{\text{rigid}}\delta^2\omega_D^2\left(\frac{Z}{A}\right)^2\xi\,[\mu_N^2\,\text{MeV}], \quad (13)$$

$$S_{-1} = \frac{3}{16\pi}\Theta_{\text{rigid}}\left(\frac{2Z}{A}\right)^2[\mu_N^2\ \text{MeV}^{-1}], \quad (14)$$

where Θ_{rigid} is the rigid moment of inertia, ξ the reduction factor, and ω_D the isovector giant dipole resonance IVGDR frequency. The nuclear quadrupole deformation $\delta = 0.27$ is obtained using the ground state deformation parameter β_2. To lowest order the two quantities are proportional: $\delta \approx \beta_2\sqrt{45/(16\pi)}$. The ground state deformation taken is the average of the RIPL tabulated value [13] for ^{242}Pu and ^{244}Pu ($\beta_2 = 0.29$) and from a microscopic calculation [40] ($\beta_2 = 0.28$). The two sum rules can now be utilized to extract the SR centroid ω_{SR} and strength B_{SR}:

$$\begin{aligned} \omega_{SR} &= \sqrt{S_{+1}/S_{-1}} \\ B_{SR} &= \sqrt{S_{+1}S_{-1}}. \end{aligned} \quad (15)$$

The two last columns of Table III show the predicted ω_{SR} and B_{SR} from the sum-rule estimates. Both values are in very good agreement with our measurements.

V. HAUSER FESHBACH CALCULATIONS OF THE ^{242}Pu(n,γ) CROSS SECTION WITH TALYS

The γSF is important for the description of the γ emission channel in nuclear reactions and is one of the main inputs for cross section calculations using a statistical framework. Calculations made with the TALYS code [41,42] for ^{238}Np have shown excellent agreement with measured data and that the SR can have an impact on the cross section (maximum of $\approx 25\%$ for a 1 MeV incident neutron [9]).

Unfortunately, there are no measured data for the ^{242}Pu(n,γ) reaction for neutron energies above 100 keV. A comparison of the ^{242}Pu(n,γ) cross section with the ENDF/B-VII.1 [43], JENDL-4.0 [44] and TENDL2014 [42] was done. ENDF/B-VII.1 and JENDL-4.0 are using the same models and input parameters to calculate the level density and the γSF. Figure 6 shows the level densities used by ENDF/B-VII.1, JENDL-4.0, and TENDL2014 to calculate cross sections, as well as the level density measured in the present work. TENDL2014, ENDF/B-VII.1, and JENDL-4.0 are within a factor of 2 from the measured level density in the present work.

Figure 7 shows the γSF used in ENDF/B-VII.1, JENDL-4.0 and TENDL2014 to calculate cross sections, as well as the one measured in the present work. ENDF/B-VII.1 and JENDL-4.0 reproduce correctly the measured (γ, x) data [30–32]. The low

energy region does not correspond well to the data measured in the present work. TENDL2014 does not reproduce published (γ, x) data.

To calculate the ^{242}Pu(n,γ) cross section, the observed level density and γSF (data from Figs. 3 and 4, respectively) have been used as input parameters in TALYS. The average resonance spacing D_0 and the average radiative width $\langle\Gamma_\gamma\rangle$, from Ref. [22], are reproduced by the TALYS calculation. The neutron optical potential is taken from Ref. [45].

Figure 8 shows the results of the cross-section calculations using the TALYS code with the SR (continuous red curve with blue error-band) and without (dashed red curve with red dots error-band), the ENDF/B-VII.1 (black curve), JENDL-4.0 (brown curve), and TENDL2014 (blue curve) evaluations. The error band is generated by taking into account the uncertainty in the two pygmy resonances labeled pygmy1 and pygmy2 in Fig. 4 and the average radiative width $\langle\Gamma_\gamma\rangle$. Including the SR in the calculation leads to some variations in the cross section (up to $\approx 10\%$ at 1.7 MeV). This is smaller in comparison to the recent measurement on ^{238}Np [9] with a comparable SR strength.
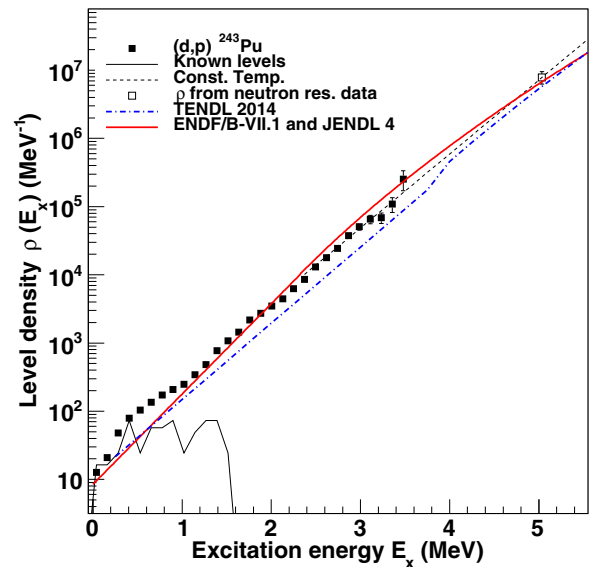

FIG. 6. Measured level density (black filled squares) compared to the level density used in ENDF/B-VII.1 [43] and JENDL-4.0 [44] (red continuous curve), and TENDL2014 [42] (blue dotted-dashed curve) calculations. The measured level density was normalized to the level density of known levels (black line) and to the level density extracted from known neutron resonance spacings D_0 [22] (empty square).
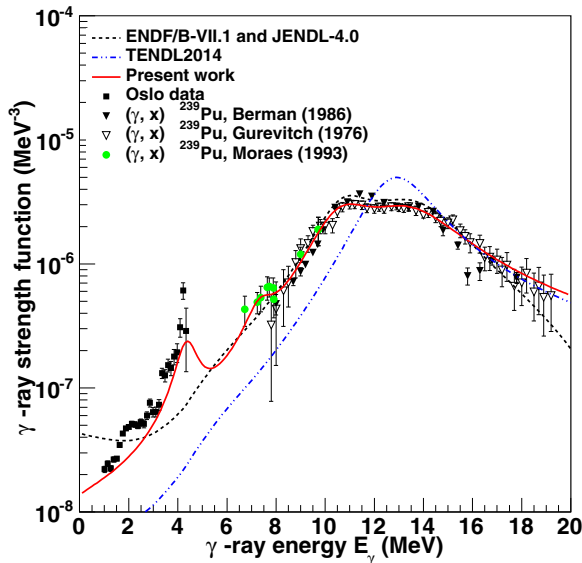
FIG. 7. Comparison between the γSF extracted in the present work (red curve) from measured data (black filled squares) and the one used in ENDF/B-VII.1 and JENDL-4.0 (dashed black curve), TENDL2014 (blue dashed-dotted curve). The (γ, x) data (black filled triangles, empty triangles, and green dots) are taken, respectively, from Berman *et al.* [30], Gurevitch *et al.* [31], and Moraes *et al.* [32].

Below 200 keV, the data libraries and our calculations agree with the direct measurement from Hockenbury *et al.* [46] (black triangles) and the cross section data from Wisshak *et al.* [47], obtained as a ratio to the ^{197}Au(n, γ) cross section.
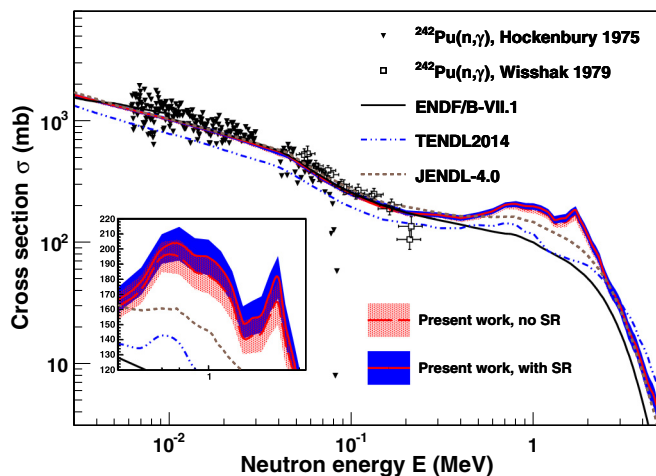
FIG. 8. Calculated ^{242}Pu(n, γ) cross section using level density and γSF parameters obtained in the present work, including the $M1$ scissors mode (continuous red curve with blue error-band) and without it (dashed red curve with red dots error-band). A zoom in the energy region 0.5 to 2 MeV, where the impact of the SR is the most important, is shown in the inset. The predictions are compared at low energy with measured data from Hockenbury *et al.* [46] (black triangles), Wisshak and Käppeler [47] (empty squares), and evaluations from ENDF/B-VII.1 (black curve), JENDL-4.0 (dashed grey curve), TENDL2014 (blue dotted-dashed curve).

The open squares are extracted using the ^{197}Au(n, γ) cross section from the IRDFF-1.05 database [48]. At higher energies, large discrepancies are observed between the different libraries and our calculation as can be expected due to the discrepancies in the level densities and γSF and the lack of directly measured experimental data at higher neutron energies. Surprisingly the ENDF/B-VII.1 and JENDL-4.0 cross sections do not match despite using the same level density and γSF. The ENDF/B-VII.1 cross section was renormalized to an integral measurement over a broad fast spectrum [49]. Direct measurements of the ^{242}Pu(n, γ) cross section are planned at the n_TOF facility at CERN and should help solve the discrepancy.

VI. CONCLUSIONS AND FUTURE WORK

The level density and γSF of ^{243}Pu have been measured in the quasicontinuum using the Oslo method. The level density follows closely a constant-temperature level density formula as seen in recent investigations of other actinides using the same method [7–9]. The γSF displays a double-humped resonance in the $E_\gamma = 1$–3.5 MeV region, interpreted as the scissors resonance. Its energy centroid and total strength are very well described by the sum-rule estimate assuming a rigid-body moment of inertia.

The observed level density and γSF have been used as inputs in Hauser-Feshbach calculations implemented in the TALYS code. Large discrepancies with the ENDF, JENDL, and TENDL databases raise the need for a direct measurement of the ^{242}Pu(n, γ) cross section.

A ^{244}Pu target has recently been made at Lawrence Livermore National Laboratory. Experiments at the Oslo Cyclotron Laboratory using the $(^3$He,$\alpha)$ and/or (p, d) entrance channels are of interest to compare with the results presented here and study the effect of spin population of the compound nucleus on the extracted statistical properties of the nucleus.

[1] M. B. Chadwick *et al.*, Nucl. Data Sheets **112**, 2887 (2011).
[2] G. Aliberti, G. Palmiotti, M. Salvatores, T. K. Kim, T. A. Taiwo, M. Anitescu, I. Kodeli, E. Sartori, J. C. Bosq, and J. Tommasi, Ann. Nucl. Energy **33**, 700 (2006).
[3] M. Arnould, S. Goriely, and K. Takahashi, Phys. Rep. **450**, 97 (2007).
[4] A. Schiller *et al.*, Nucl. Instrum. Methods Phys. Res. A **447**, 498 (2000).
[5] A. C. Larsen *et al.*, Phys. Rev. C **83**, 034315 (2011).
[6] M. Guttormsen *et al.*, Phys. Rev. Lett. **109**, 162503 (2012).
[7] M. Guttormsen *et al.*, Phys. Rev. C **88**, 024307 (2013).
[8] M. Guttormsen *et al.*, Phys. Rev. C **89**, 014302 (2014).
[9] T. G. Tornyi *et al.*, Phys. Rev. C **89**, 044323 (2014).
[10] R. A. Henderson, J. M. Gostic, J. T. Burke, S. E. Fisher, and C. Y. Wu, Nucl. Instrum. Methods Phys. Res. A **655**, 66 (2011).
[11] M. Guttormsen, A. Bürger, T. E. Hansen, and N. Lietaer, Nucl. Instrum. Methods Phys. Res. A **648**, 168 (2011).
[12] M. Guttormsen *et al.*, Phys. Scr. T **32**, 54 (1990).
[13] R. Capote *et al.*, Reference Input Library, RIPL-2 and RIPL-3, available online at http://www-nds.iaea.org/RIPL-3/.
[14] C. D. Nesaraja and E. A. McCutchan, Nucl. Data Sheets **121**, 695 (2014).
[15] M. Guttormsen, T. S. Tveter, L. Bergholt, F. Ingebretsen, and J. Rekstad, Nucl. Instrum. Methods Phys. Res. A **374**, 371 (1996).
[16] M. Guttormsen, T. Ramsøy, and J. Rekstad, Nucl. Instrum. Methods Phys. Res. A **255**, 518 (1987).
[17] E. Fermi, *Nuclear Physics* (University of Chicago Press, Chicago, 1950).
[18] D. M. Brink, Ph.D. thesis, Oxford University, 1955.
[19] Data extracted using the NNDC On-Line Data Service from the ENSDF database, August 2015.
[20] T. Ericson, Nucl. Phys. **11**, 481 (1959).
[21] T. von Egidy and D. Bucurescu, Phys. Rev. C **72**, 044311 (2005); **73**, 049901(E) (2006).
[22] S. F. Mughabghab, *Atlas of Neutron Resonances*, 5th ed. (Elsevier Science, New York, 2006).
[23] T. E. Young and S. D. Reeder, Nucl. Sci. Eng. **40**, 389 (1970).
[24] E. Rich, A. Tudora, G. Noguere, J. Tommasi, and J. F. Lebrat, Nucl. Sci. Eng. **162**, 178 (2009).
[25] F. Zeiser (unpublished).
[26] A. Gilbert and A. G. W. Cameron, Can. J. Phys. **43**, 1446 (1965).

[27] M. Guttormsen *et al.*, Eur. Phys. J. A **51**, 170 (2015).
[28] A. Voinov, M. Guttormsen, E. Melby, J. Rekstad, A. Schiller, and S. Siem, Phys. Rev. C **63**, 044313 (2001).
[29] J. Kopecky and M. Uhl, Phys. Rev. C **41**, 1941 (1990).
[30] B. L. Berman, J. T. Caldwell, E. J. Dowdy, S. S. Dietrich, P. Meyer, and R. A. Alvarez, Phys. Rev. C **34**, 2201 (1986).
[31] G. M. Gurevich, L. E. Lazareva, V. M. Mazur, G. V. Solodukhov, and B. A. Tulupov, Nucl. Phys. **273**, 326 (1976).
[32] M. A. P. De Moraes and M. F. Cesar, Phys. Scr. **47**, 519 (1993).
[33] W. Thomas, Naturwissenschaften **13**, 627 (1925).
[34] F. Reiche and W. Thomas, Z. Phys. **34**, 510 (1925).
[35] W. Kuhn, Z. Phys. **33**, 408 (1925).
[36] M. Herman, R. Capote, B. V. Carlson, P. Oblozinsky, M. Sin, A. Trkov, H. Wienke, and V. Zerkin, Nucl. Data Sheets **108**, 2655 (2007).
[37] E. B. Balbutsev, I. V. Molodtsova, and P. Schuck, Phys. Rev. C **91**, 064312 (2015).
[38] E. Lipparini and S. Stringari, Phys. Rep. **175**, 103 (1989).
[39] J. Enders, P. von Neumann-Cosel, C. Rangacharyulu, and A. Richter, Phys. Rev. C **71**, 014306 (2005).
[40] S. Goriely, N. Chamel, and J. M. Pearson, Phys. Rev. Lett. **102**, 152503 (2009).
[41] A. J. Koning, S. Hilaire, and M. C. Duijvestijn, TALYS-1.0, in *Proceedings of the International Conference on Nuclear Data for Science and Technology, 22–27 April 2007, Nice, France*, edited by O. Bersillon, F. Gunsing, E. Bauge, R. Jacqmin, and S. Leray (EDP Sciences, 2008), p. 211, http://www.talys.eu/.
[42] A. J. Koning and D. Rochman, Nucl. Data Sheets **113**, 2841 (2012).
[43] M. B. Chadwick *et al.*, Nucl. Data Sheets **107**, 2931 (2011).
[44] K. Shibata *et al.*, J. Nucl. Sci. Technol. **48**, 1 (2011).
[45] E. S. Sukhovitskiĭ, S. Chiba, J. Lee, O. Iwamoto, and T. Fukahori, J. Phys. G: Nucl. Part. Phys. **30**, 905 (2004).
[46] R. W. Hockenbury, A. J. Sanislo, and N. N. Kaushal, Conference on Nuclear Cross Sections and Technology, Washington, Vol. 2, p. 584 (1975).
[47] K. Wisshak and F. Käppeler, Nucl. Sci. Eng. **69**, 39 (1979).
[48] V. G. Pronyaev and K. I. Zolotarev, IRDFF-1.05 MAT 7925, May 2008.
[49] A. A. Druzhinin, V. K. Grigor'ev, A. A. Lbov, S. P. Vesnovskii, N. G. Krylov, and V. N. Polynov, Atomnaya Energiya **42**, 314 (1977).